The 2012 World Congress on
Advances in Civil, Environmental, and Materials Research (ACEM' 12)
Seoul, Korea, August 26-30, 2012

Hot Workability of Extruded AZ31 Magnesium Alloy Containing 1.5% Nano-alumina

T. Zhong[1)], K.P. Rao[2)], Y.V.R.K. Prasad[3)], M. Gupta[4)]

[1) 2)] *Department of Mechanical and Biomedical Engineering, City University of Hong Kong, 83 Tat Chee Avenue, Kowloon, Hong Kong SAR, China*
[3)] *Consultant, processingmaps.com (formerly with City University of Hong Kong)*
[4)] *Department of Mechanical Engineering, National University of Singapore, 9 Engineering Drive 1, Singapore 117575, Singapore*

[1)] *tzhong3@student.cityu.edu.hk*

ABSTRACT

Mg-3Al-1Zn (AZ31) is one of the most widely used wrought magnesium alloys for applications that demand light-weight structural components. Microstructural refinement through thermo-mechanical means is an effective way of improving strength and ductility of the alloys, but refined microstructures are susceptible to grain coarsening at high temperature. Thus, microstructure control and stability at application temperature is critical to properties of final products. These objectives may be achieved by incorporating a small quantity of nano sized particles in bulk alloys to form composites. Nano-alumina particulates exhibit an excellent combination of specific stiffness, high temperature mechanical properties and oxidation resistance. In this research, the hot workability of AZ31 alloy containing 1.5 vol. % of nano-alumina was studied using processing maps. It was found that microstructure stability of the alloy has substantially improved. The grain size of AZ31 was basically small for most of the compression conditions (temperature and strain rate) employed in this research.

1. INTRODUCTION

Magnesium alloys are favored for various components in auto and aerospace industries due to their low density, superior damping capacity, and high specific strength. Among these alloys AZ31 (Mg-3Al-1Zn) is probably the most favored wrought magnesium alloys, and it has been extensively investigated. However, such

[1)] Graduate Student
[2)] Associate Professor and Associate Head
[3)] Consultant
[4)] Associate Professor

alloys have the limited workability of at room temperature due to insufficient slip systems. Thus, metal forming is usually done at elevated temperature, where additional slip systems will be activated (Lapovok 2004, Letzig 2006, Uematsu 2006).Microstructural refinement is an effective way to improve strength and ductility of the alloys, but thermo-mechanically refined microstructures are susceptible to coarsening and instability at high temperature (Kim 2004,). The addition of nano-particle dispersoids is being considered for achieving microstructural refinement and strengthening (Lukac 2005, Wong 2007, Hassan 2008). In the raw material preparation stage of this research, a new material synthesis method, named disintegrated melt deposition (DMD), was applied (Hassan 2007). This technique would help not only in refining the microstructure of the billet but also in distributing nano-dispersoids uniformly in the microstructure of the composite. Earlier, the hot working characteristics of a Mg-1 vol. % nano alumina composite have been evaluated (Prasad 2009). The composite may be hot worked at higher strain rates similar to the base Mg material, but at lower strain rates the apparent activation energy for hot working is much higher than in the matrix material. The nano alumina particles have a tendency to migrate preferentially to the prior particle boundaries of the composite and stabilize them from migration. The aim of this research is to investigate microstructure evolution of AZ31-1.5 vol. % nano alumina composite (AZ31-NAL) during hot working with a view to find safe and optimum workability window for this composite and also to design methods that assist microstructural control during the secondary-forming stage.

The principles and basis for processing maps are briefly introduced here. Processing map is an explicit representation of the response of a material, in terms of microstructure mechanisms, to the imposed processing parameters and consists of a superimposition of a power dissipation map and an instability map. These are developed on the basis of the Dynamic Materials Model, which is essentially a continuum model using the concepts of systems engineering, extremum principles of irreversible thermodynamics with application to continuum mechanics of large plastics flow and those describing the stability and self organization of chaotic systems (Prasad 1997). The efficiency of power dissipation occurring through microstructural changes during deformation as a function of temperature and strain rate is given by

$$\eta = \frac{2m}{m+1} \tag{1}$$

In the Eq. (1), *m* is strain rate sensitivity. The efficiency variation of power dissipation with temperature and strain rate represents a power dissipation map, which is generally viewed as an iso-efficiency contour map. This efficiency η represents the relative rate of internal entropy production during hot deformation and characterizes the dissipative microstructure change under different temperature and strain rate. In addition, the extremum principles of irreversible thermodynamics as applied to continuum mechanics of large plastic flow (Prigogine 1970) are explored to define a criterion for the onset of flow instability given by the equation for the instability parameter

$$\xi(\dot{\varepsilon}) = \frac{\partial \ln[m/(m+1)]}{\partial \ln \dot{\varepsilon}} + m \leq 0 \tag{2}$$

In the Eq. (2), *m* is strain rate sensitivity and $\dot{\varepsilon}$ is strain rate. This formula could be physically interpreted in simple term as follows: if the material system does not produce entropy constitutively at a rate that at least matches the rate of entropy input through imposed parameters, the flow becomes localized and cause flow instability, where $\xi(\dot{\varepsilon}) \leq 0$ (Prasad 1997). Combing an instability map with a corresponding power dissipation map could make a processing map, which helps to identify temperature-strain domains where workability of a material is optimal, such as dynamic recrystallization (DRX) and also to avoid regimes of flow instabilities, such as flow localization.

2. MATERIAL AND EXPERIMENTAL PROCEDURE

AZ31–1.5 vol. % nano alumina composite was prepared by Disintegrated Melt Deposition (DMD) technique. In primary processing, synthesis of this composite material involved heating the magnesium alloy pieces to 750 ^{o}C and stirring in an inert Ar gas atmosphere in a graphite crucible. The composite melt slurry was subsequently deposited onto a metallic substrate and billets of 40 *mm* diameter were obtained. In the secondary processing, the deposited billets were soaked for 1 hour at a temperature of 400 ^{o}C before extrusion and then hot extruded through a die preheated to 350 ^{o}C using an extrusion ratio of 12.96:1 to produce rods of 9.8 *mm* diameter. During this process, colloidal graphite was used as lubricant.

Cylindrical specimens of 9.8 *mm* diameter and 15 *mm* height were machined from the extruded rods for isothermal uniaxial compression along the direction of extrusion. For inserting a thermocouple to measure the instantaneous specimen temperature during deformation, a hole of 1 *mm* diameter and 4.9 *mm* depth was machined at mid-height to reach the center of the specimen.

Conditions for the isothermal uniaxial compression were as follows: Strain rates in a range of 0.0003-10 s^{-1} and temperatures in a range of 250-500 ^{o}C. Graphite powder mixed with grease was used as the lubricant in the experiments. The specimens were deformed up to a true strain of 1 and then quenched in water. The load-stroke data were converted into true stress-true strain curves. The flow stress values were corrected for the adiabatic temperature rise. The deformed specimens were sectioned in the center parallel to the compression axis and the cut surface was mounted, polished and etched for metallographic examination. Picric acid and acetic acid based solution was used for etching the polished surface to reveal the microstructure.

3. RESULTS AND DISCUSSION

3.1. Stress-strain Curves

The flow curves obtained for 450 ^{o}C at different strain rates are shown in Fig. 1. The flow curves obtained at strain rates of 10 and 1 s^{-1} exhibit significant work softening which is less for lower strain rates. It is commonly believed that DRX is one of the mechanisms responsible for the flow softening behavior since it softens the material through nucleation of grains followed by grain boundary migration. When steady-state is reached, the rate of nucleation and the rate of migration will balance each other. Temperature corrected compressive flow stress (MPa) of AZ31-NAL alloy at a strain of 0.5 in the strain rate range 0.0003-10 s^{-1} and temperature range 250-500 ^{o}C is shown in Table 1.

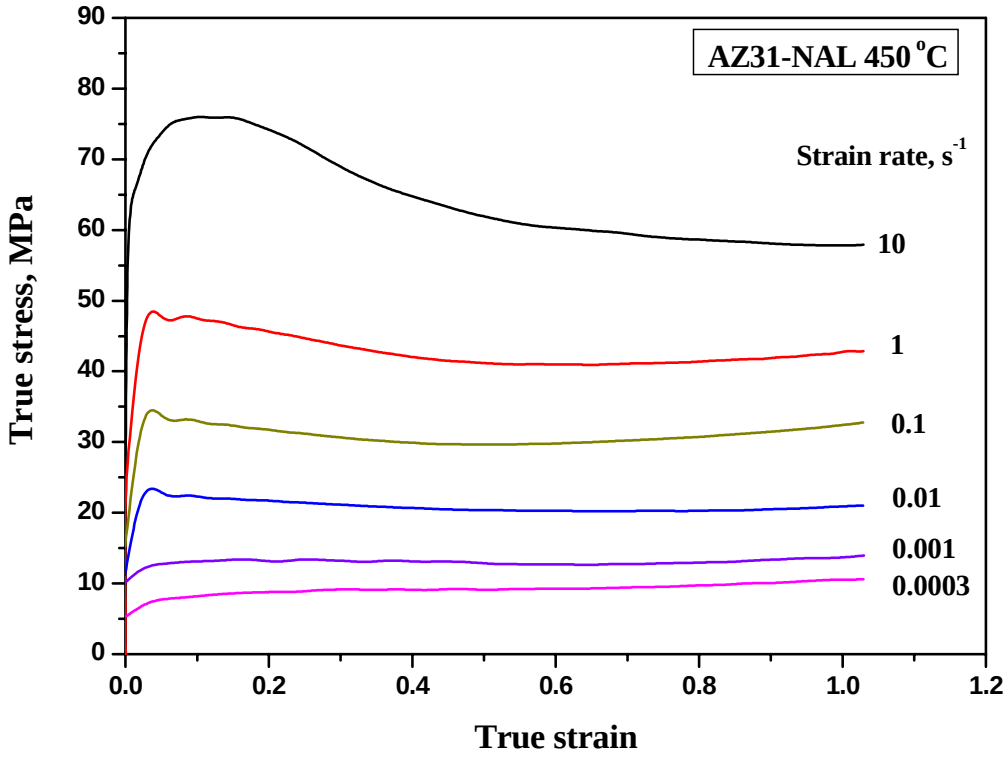

Fig. 1: Stress-strain curves of AZ31-NAL at temperatures of 450 °C obtained in uniaxial compression at different strain rates.

Table 1: Temperature corrected compressive flow stress (MPa) of AZ31-NAL alloy at a strain of 0.5 at different strain rates and temperatures.

Strain rate, s^{-1}	Temperature, °C					
	250	300	350	400	450	500
10	214.6	173.7	120.2	85.8	65.2	48.3
1	160.6	120.5	78.6	60.4	45.2	32.5
0.1	105.2	75.3	57.4	43.6	31.6	22.2
0.01	77.3	54.8	40.1	28.5	20.4	13.9
0.001	56.1	37.6	26.6	17.7	12.8	8.4
0.0003	45.8	30.1	22.1	14.4	9.1	7.0

3.2. Processing Map and Microstructures

The processing map developed at strains of 0.5 on the basis of the Eqs. (1) and (2) is shown in Fig. 2. The map exhibits two domains in lower strain rate range: Domain #1 in the temperature range of 250–350 °C and strain rate range of 0.0003-0.01 s^{-1} with a peak efficiency of about 31% occurring at 300 °C/0.0003 s^{-1}, and Domain #2 in the temperature range of 380–500 °C and strain rate range of 0.0003-0.01 s^{-1} with a peak efficiency of about 43% occurring at 450 °C/0.0003 s^{-1}. In addition, a third domain is found at the temperature range of 300-400 °C and strain rate range of 1-10 s^{-1} with a peak efficiency of around 32% occurring at 350 °C/10 s^{-1}.

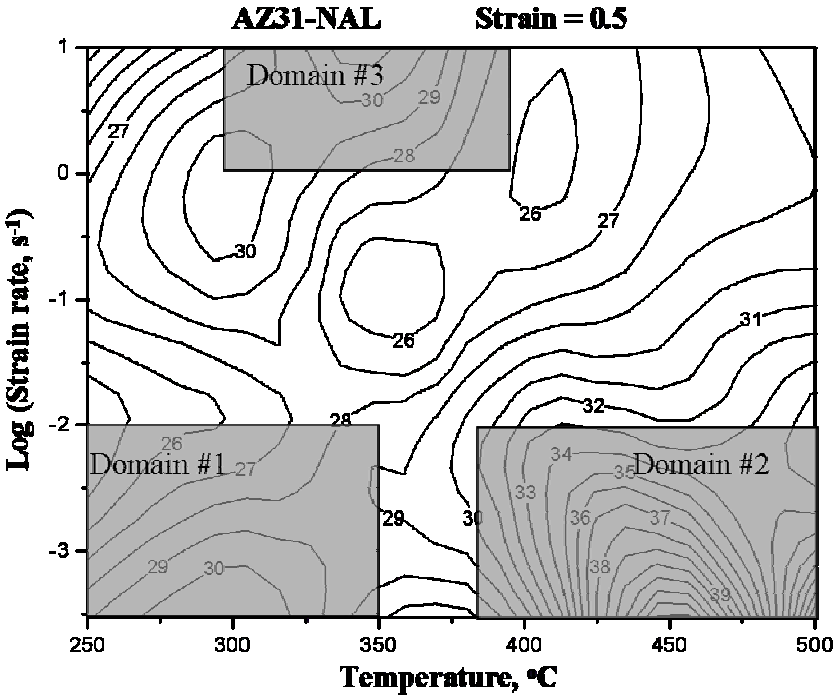

Fig. 2: Processing map of AZ31-NAL at compression strain of 0.5. The numbers against the contours represent efficiency of power dissipation in percentage.

The microstructure obtained on specimen deformed at 300 ^{o}C/0.0003 s^{-1} corresponding to the peak efficiency in Domain #1, is shown in Fig. 3. This exhibits fine dynamically recrystallized grain structure suggesting that DRX is occurring in this domain. The conditions of this domain will therefore result in good workability and a fine grain microstructure.

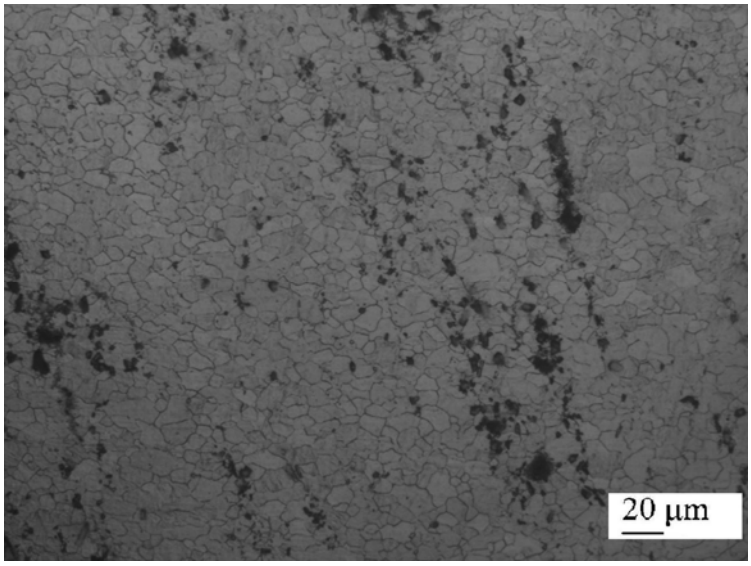

Fig. 3: Microstructure obtained on the specimen deformed at 300 ^{o}C/ 0.0003 s^{-1}.

The microstructure obtained at the peak efficiency condition in Domain #2, is shown in Fig. 4. The grain structure looks recrystallized and many of the boundaries are oriented at 45^{o} with respect to the compression axis. Such a configuration will promote sliding of the boundaries since a shear stress is resolved along them. Since

grain boundary sliding is a viscous process, it will exhibit higher strain rate sensitivity or higher efficiency of power dissipation (43% in this case). Grain boundary sliding will result in wedge cracking or superplasticity if the wedge cracks are repaired by accommodation of stress concentration by diffusional flow or plastic deformation.

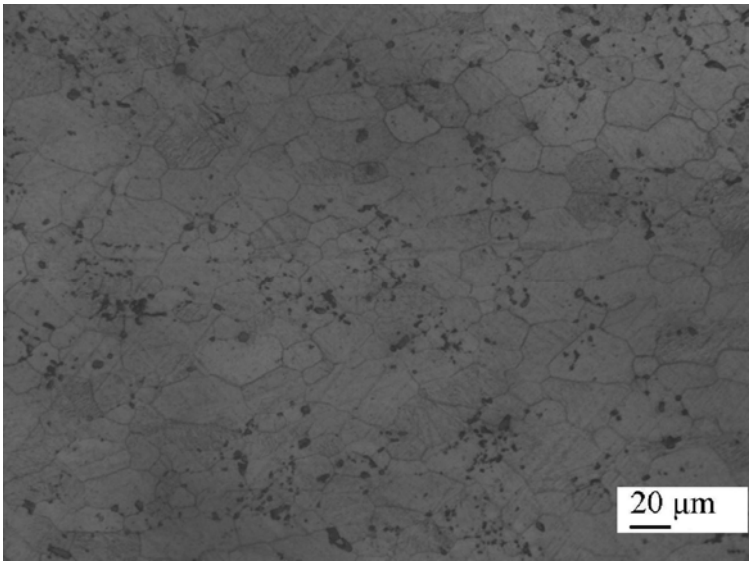

Fig. 4: Microstructure obtained on the specimen deformed at 450 ^{o}C/ 0.0003 s^{-1}.

The microstructure of the specimen deformed under peak efficiency conditions in Domain #3 is shown in Fig. 5, which reveals fine grained recrystallized microstructure suggesting that this is also a DRX domain. Two DRX domains located one at lower strain rates and the other at higher strain rates have been reported earlier in wrought AZ31 alloy (Prasad 2008).

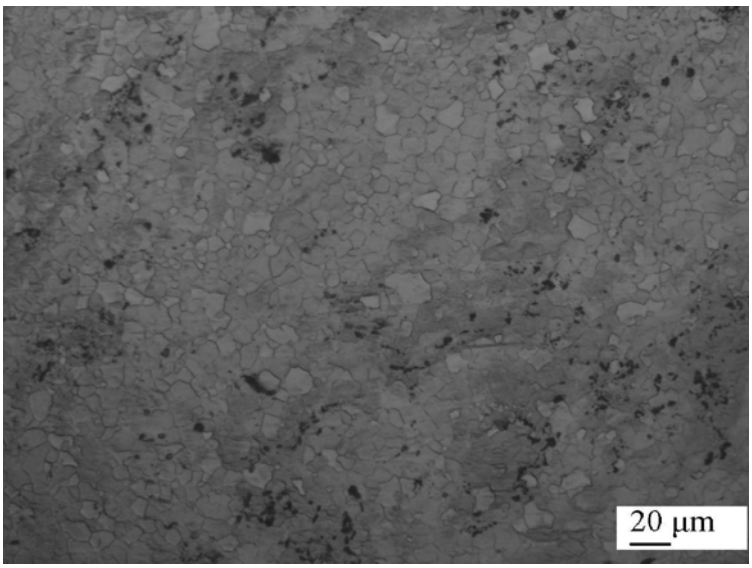

Fig. 5: Microstructure of the specimen deformed at 350 ^{o}C/10 s^{-1} (Domain #3).

The average grain sizes measured on all the compressed samples are given in Table 2. It can be seen that though the grain size increases with temperature, there is no simple relationship with strain rate. This is mainly attributed to the separation of different workability domains and bifurcations between boundaries.

Table 2: Average grain sizes in *μm* measured on AZ31-NAL specimens deformed in hot compression at different temperatures and strain rates.

Strain rate,s^{-1}	Temperature, ^oC					
	250	300	350	400	450	500
10	6.7	9.5	10.2	13.8	15.8	18.9
1	8.1	10.4	11.1	20.1	25.6	33.3
0.1	7.2	11.2	18.5	31.2	71.5	98.7
0.01	6.1	6.9	9.8	10.2	14.5	22.8
0.001	6.9	7.2	10.7	12.8	19.5	25.6
0.0003	7.1	10.7	13.3	20.8	33.3	41.6

4. CONCLUSIONS

On the basis of processing maps, kinetic analysis, microstructural features, the following conclusion are drawn on the hot working characteristics of AZ31-NAL material produced by disintegrated metal deposition (DMD) technique:

(a) The processing map exhibits 3 domains in the temperature and strain rate ranges — Domain #1: 250-350 ^oC and 0.0003-0.01 s^{-1}, Domain #2 380-500 ^oC and 0.0003-0.01 s^{-1}, and Domain #3: 300-400 ^oC and 1-10 s^{-1}.
(b) Dynamic recrystallization (DRX) occurs in domains #1 and #3 resulting in fine grained microstructures.
(c) In domain #2, grain boundary sliding occurs leading to wedge cracking in compression.
(d) Hot working the material may be conducted safely in both domains #1 and #3, although domain #3 is preferable due to its higher strain rate range.
(e) While the grain size increases with deformation temperature, the abnormal grain sizes found with respect to strain rate are due to bifurcations between the different workability domains in the processing map.

ACKNOWLEDGEMENT

The work presented in this paper has been supported by a strategic research grant from City University of Hong Kong (Project No. 7008098) and a grant from the Research Grants Council of the Hong Kong Special Administrative Region, China (Project No. 114811).

REFERENCES

S.F. Hassan, M. Gupta (2007), “Development of nano-Y2O3 containing magnesium nanocomposites using solidification processing,” *J. All. Compds*., Vol. **429**, 176-183.
S.F. Hassan, M.J. Tan, M. Gupta (2008), “High-temperature tensile properties of Mg/Al2O3 nanocomposite,” *Mater. Sci. Eng. A,* Vol. **486**, 56-62.
H.K. Kim, W.J. Kim (2004), “Microstructural instability and strength of an AZ31 Mg alloy after severe plastic deformation,” *Mater. Sci. Eng. A,* Vol. **385**, 300-308.

R.Ye. Lapovok, M.R. Barnett, C.H.J. Davies, J (2004), “Construction of extrusion limit diagram for AZ31 magnesium alloy by FE simulation,” *J. Mater. Proc. Technol.,* Vol. **146**, 408-414.
D. Letzig, J. Swiostek, J. Bohlen, P.A. Beaven, M.O. Pekguleryuz, L.W.F. Mackenzie (Eds.) (2006), “Magnesium Wrought Alloy Properties of the AZ-Series,” Metallurgy and Petroleum, Canadian Institute of Mining, Montreal, Canada, pp. 569-580.
P. Lukac, Z. Trojanova (2005), “Magnesium-based nanocomposites,” *Int. J. Mater. Product Tech.*, Vol. **23**, 121-137.
Y.V.R.K. Prasad, K.P. Rao (2008), “Processing maps for hot deformation of rolled AZ31 magnesium alloy plate: Anisotropy of hot workability,” *Mater. Sci. Eng. A,* Vol. **487**, 316–327.
Y.V.R.K. Prasad, K.P. Rao, M. Gupta (2009), “Hot workability and deformation mechanisms in Mg/nano–Al2O3 composite,” *Comp. Sci.Technol.,* Vol. **69**, 1070-1076.
Y.V.R.K. Prasad, S. Sasidhara (1997), “Hot working Guide: A compendium of Processing Maps,” ASM International, Materials Park, OH, pp 3-24.
I. Prigogine (1970), “Time, structure, and fluctuations,” *Science*, Vol. **201**, 777-787.
Y. Uematsu, K. Tokaji, M. Kamakura, K. Uchida, H. Shibata, N. Bekku (2006), “Effect of extrusion conditions on grain refinement and fatigue behaviour in magnesium alloys,” *Mater. Sci. Eng. A,* Vol. **434**, 131-140.
W.L.E. Wong, M. Gupta (2007), “Improving Overall Mechanical Performance of Magnesium Using Nano-Alumina Reinforcement and Energy Efficient Microwave Assisted Processing Route,” *Adv. Eng. Mater.,* Vol. **9**, 902-909.